Effect of pH on the Formation of Gibbsite-Layer Films at the Muscovite (001)−Water Interface

Lee, S. S.; Schmidt, M.; Sturchio, N. C.; Nagy, K. L.; Fenter, P.;

Originally published:

February 2019

Journal of Physical Chemistry C 123(2019)11, 6560-6571

DOI: https://doi.org/10.1021/acs.jpcc.8b12122

Effect of pH on the Formation of Gibbsite-Layer Films at the Muscovite (001)−Water Interface

Sang Soo Lee,[1,*] Moritz Schmidt,[2] Neil C. Sturchio,[3] Kathryn L. Nagy,[4] and Paul Fenter[1]

[1] Chemical Sciences and Engineering Division, Argonne National Laboratory, 9700 South Cass Avenue, Lemont, IL 60439, United States

[2] Helmholtz-Zentrum Dresden-Rossendorf, Institute of Resource Ecology, Dresden, Germany

[3] Department of Geological Sciences, University of Delaware, Newark, DE 19716, United States

[4] Department of Earth and Environmental Sciences, 845 West Taylor Street, MC-186, University of Illinois at Chicago, Chicago, IL 60607, United States

* Corresponding author: phone: (630)252-6679; fax: (630)252-9570; e-mail: sslee@anl.gov

ABSTRACT: Aluminum (oxy)hydroxide films play an important role as sorbents of toxic elements in aqueous environments, where their heterogeneous nucleation and growth can be controlled by the speciation of dissolved Al species and the charge and structure of underlying mineral surfaces. The structure of gibbsite films nucleated at the interface between the muscovite (001) surface and 1 mM $AlCl_3$ solutions was investigated as a function of pH using *in situ* X-ray reflectivity. Growth of well-ordered gibbsite films was observed at pH 3–4, even when the solutions were undersaturated with respect to gibbsite. The ordering of these gibbsite films likely resulted from the structural similarity (i.e., epitaxy) between the basal planes of gibbsite and muscovite. In contrast, no film growth was observed at pH 9−12 where the solutions were supersaturated with respect to gibbsite. These results indicate that adsorption and accumulation of aqueous Al(III) species (i.e., Al^{3+} and $AlOH^{2+}$ at acidic pH) is a critical step for the formation of secondary minerals on the negatively-charged muscovite surface.

1. Introduction

Aluminum plays an important role in controlling geochemical reactions in near-surface environments.[1-7] Aluminum-bearing minerals and dissolved aluminum readily undergo hydrolysis, affecting the acidity of soils and natural waters. Most Al ions dissolved in natural waters exist as aqueous complexes or clusters, which can precipitate as secondary aluminum (oxy)hydroxide minerals.[2,4,8-12] These minerals usually form on the walls of pores and cracks, thereby interacting directly with pore water and affecting the mobility of dissolved nutrients[13-15] and toxic elements.[16-21] They also exist in storage sites for nuclear waste sites, potentially influencing the fate of radioactive elements.[22-25] In particular, gibbsite, α-$Al(OH)_3$, has been found as a common mineral in these sites, hence the reaction mechanisms of gibbsite with radioactive ions have been widely investigated.[26-30] For example, adsorption of U(VI) onto gibbsite was studied in 0.1 M $NaClO_4$ background electrolyte solutions at near-neutral to basic pH (from 5.0 to 10) using time-resolved laser-induced fluorescence spectroscopy (TRLFS) and extended X-ray absorption fine structure (EXAFS) measurements.[26-28] Two adsorbed uranyl (UO_2^{2+}) species were identified as bidentate mononuclear inner-sphere (IS) and polynuclear uranyl surface complexes.[28] In addition, some U species adsorbed on gibbsite surfaces were observed to exist as carbonate complexes by *in situ* time-resolved attenuated total reflection Fourier-transform infrared (ATR FTIR) and EXAFS spectroscopies at similar pH.[29-30]

Gibbsite is also an important phase in the aluminum production industry. The formation of gibbsite from supersaturated aluminate solutions is the key step during the Bayer process for alumina and aluminum production. However, it is also the slowest stage in the process, leading to significant operating costs. The nucleation and growth of gibbsite is reported to be extremely slow in solutions[31-32] and is normally considered to be controlled by surface reactions.[33-35] Hence,

additives have been widely used as seeding materials to increase gibbsite growth rates as well as to control the size and morphology of the particles.[36-40]

Heterogeneous nucleation of gibbsite and other Al (oxy)hydroxide phases has been studied in basic solutions simulating the conditions in some industrial processes. For example, the formation of aluminum hydroxide ($Al(OH)_3$) phases on lepidocrocite and ferrihydrite substrates was studied in a supersaturated sodium aluminate liquor at 70 °C using *in situ* X-ray diffraction. Several types of $Al(OH)_3$ polymorphs formed, including gibbsite, bayerite, and nordstrandite, among which gibbsite was dominant presumably because of its structural similarity to the seeding materials, especially to the lepidocrocite substrate.[41] The morphological evolution of gibbsite crystals during homoepitaxial growth was studied in basic sodium and potassium aluminate solutions using atomic force microscopy (AFM). The Burton–Cabrera–Frank (BCF) type growth mode, where nucleation and growth are initiated on steps, was the major formation mechanism for the gibbsite growth in these systems. On a perfectly smooth surface, gibbsite crystals mostly grew as isotropic two-dimensional islands, as explained by a birth and spread model.[35,39]

The nucleation and growth of gibbsite was also observed on the basal surface of muscovite mica at mildly acidic pH.[42] A freshly cleaved muscovite (001) surface was reacted with a 1 mM $Al(NO_3)_3$ solution supersaturated with respect to gibbsite at pH 3 at 80 °C for up to 47 days. The saturation index (β) of the solution was ~1.3 where β is defined as,

$$\beta = \log_{10}(IAP/K_{sp}) \quad (1)$$

with the ion activity product (IAP) and equilibrium solubility product K_{sp} of solid phase gibbsite calculated based on the reaction

$$Al^{3+} + 3H_2O = Al(OH)_3 + 3H^+ \quad (2).$$

Ex situ AFM observations showed diverse growth morphologies of the gibbsite crystals on the muscovite mica surface ranging from elongated crystals approximately 3–4 nm high, 10–20 nm wide, and 50–80 nm long to larger platelets 3–4 nm thick and up to a few μm wide. These overgrowths occurred mostly in two preferred orientations, implying an epitaxial relationship with the muscovite surface. Structural controls of the muscovite substrate on the heteroepitaxial nucleation and crystallization of gibbsite were further explored using *ex situ* AFM combined with *in situ* high-resolution X-ray reflectivity (XR).[43] These experiments were conducted with a 0.1 mM $AlCl_3$ solution that was slightly supersaturated with respect to gibbsite (with β of ~0.7) at pH 4.2. Atomic force micrographs showed the initial stage of Al hydroxide nuclei, mostly ≤1 nm high and ~10 nm wide, formed at the muscovite (001)–solution interface. *In situ* XR data indicated that these nanoparticles had an internal atomic structure that was consistent with a single gibbsite layer. The chemical identity of these nanoparticles was confirmed by probing the distribution of Ga substituted for Al at the interface using element-specific resonant anomalous X-ray reflectivity (RAXR). These results clearly demonstrated that the structure of the muscovite (001) surface controls the growth of gibbsite from Al-rich solutions.

Here, we explore the nucleation and growth of gibbsite films at the muscovite (001)–solution interface over a wide range of pH conditions. Solution pH controls the hydrolysis of dissolved Al species and the stability of solid Al (oxy)hydroxide phases. A simple expression of the monomeric Al hydrolysis can be written as,

$$Al^{3+} + nOH^- \rightarrow Al(OH)_n^{3-n} \text{ where } n = 0, 1, 2, 3, \text{ and } 4 \qquad (3)$$

where changes in the charge of Al species are expressed with respect to the degree of hydroxylation. However, this reaction does not convey the associated structural changes in coordination around dissolved Al. For example, fully hydrated Al^{3+} has an octahedral coordination geometry whereas $Al(OH)_4^-$ has a tetrahedral coordination geometry.[44] Therefore, the stepwise hydrolysis reactions

between these two end-members require the transformation of the coordination structure.[44] Furthermore, a number of spectroscopic studies have revealed the presence of oligomeric Al species[45-49] and Al oxyhydroxide clusters,[10-12] whose formation and stability can be influenced by solution pH. In contrast to the high sensitivity of Al to solution pH, the basal surface of muscovite, consisting of a plane of oxygen atoms, is largely independent of pH in terms of its structure and charge.[50-51] It has a negative structural charge (~1 e^-/A_{UC} where A_{UC} represents the area of the unit cell in the (001) surface plane of muscovite, ~47 $Å^2$)[52] that can attract cations in solution.

The charge of the dominant Al species in solution influences the adsorption strength and amount of Al(III) cations adsorbed on the muscovite. For example, trivalent cationic species Al^{3+} likely adsorbs more strongly to the negatively charged muscovite surface because of stronger electrostatic attraction than divalent or monovalent cationic species $AlOH^{2+}$ or $Al(OH)_2^+$. On the other hand, the adsorbed coverage of Al^{3+} is expected to be lower than those of $AlOH^{2+}$ or $Al(OH)_2^+$, assuming that the adsorption is driven simply for charge compensation. At acidic pH, adsorption of Al may also be affected by competitive adsorption of hydronium. At basic pH, most Al forms anionic species $Al(OH)_4^-$. Adsorption of anions on the muscovite surface via cation bridging has been proposed,[53] but the structure of this adsorbate has yet to be determined experimentally.[54] Solution pH also determines the saturation state of solid Al (oxy)hydroxide phases. At a constant dissolved Al concentration, β of gibbsite is highest at circumneutral pH values, and it decreases with both increasing and decreasing pH. The sign of β controls the stability of the solid phase and the magnitude determines the rates of precipitation and dissolution reactions in solution.[55] Likewise, the growth and dissolution of gibbsite films at the muscovite–solution interface can also be controlled by β.

The heterogeneous nucleation and growth of gibbsite films at the muscovite (001)–solution interface was measured using *in situ* XR with varying pH. These structural changes at the interface

are discussed in terms of changes in aqueous Al species and their electrostatic interactions with the negatively charged muscovite surface. Dissolution of the gibbsite overgrowth film was also performed to evaluate the thermodynamic stability of this mineral phase in solutions undersaturated with respect to gibbsite.

2. Materials and Methods

2.1. Sample preparation

The experimental solutions were prepared using two ~100 mM $AlCl_3$ stock solutions at pH 1 and 13, made by dissolving Al chloride salt (>99.99%; Sigma Aldrich Inc.) in 100 mM hydrochloric acid (HCl) and in 100 mM sodium hydroxide (NaOH). The stock solutions were diluted with deionized water (DIW) to prepare 1 mM $AlCl_3$ at pH of 2–4 and pH of 9–12. Solution pH was adjusted using 10–100 mM NaOH or HCl. Hereafter; these solutions containing 1 mM Al are labelled as "Al" followed by the solution pH, e.g., "Al3" for the 1 mM $AlCl_3$ solution at pH 3.

The chemical speciation of Al in solution was calculated using the Geochemist's Workbench® software package with the Minteq database.[56] The uncertainties of thermodynamic parameters for aqueous Al species and Al (oxy)hydroxide phases are unreported in the database. All solutions were assumed to be equilibrated with atmospheric CO_2, i.e., $pCO_2(g)$ = ~400 ppm. The Al speciation in acidic solutions was dominated by Al^{3+}, with a minor amount of $AlOH^{2+}$ (e.g., ~6% at pH 4), whereas that of the basic solutions was dominated by $Al(OH)_4^-$ (Fig. 1 and Table S1 of the Supporting Information). Solutions at pH ≥ 4 were supersaturated with respect to gibbsite and diaspore. The highest β values for gibbsite, $Al(OH)_3$, and diaspore, AlO(OH), of 3.2 and 4.1 were found at pH 9 (i.e., Al9). All solutions were undersaturated with respect to amorphous Al hydroxide, $Al(OH)_3$(am), except the Al9 solution where β of $Al(OH)_3$(am) was 0.2 (Fig. 2 and Table S2). In Al9, we observed homogeneous precipitation of solid phases after the preparation of the solution, indicating that the solution had a lower dissolved Al content than as prepared. For example, the calculated concentration of dissolved Al(III) in solution equilibrated with

$Al(OH)_3$(am) was 0.7 mM.[56] The actual concentration could be significantly lower depending on the precipitated phases, which were not identified in our study. These solid particles were filtered using a 0.1 μm porous membrane before reacting the solution with muscovite. No precipitation was observed in the other solutions. All solutions were prepared within 24 h of their reaction with muscovite.

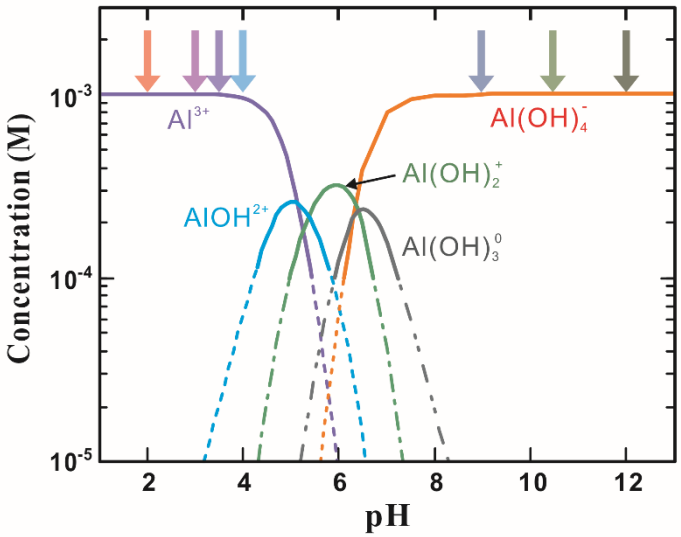

Figure 1. Speciation calculation of aqueous Al(III) as a function of pH. The thick vertical arrows indicate the pH values of solutions where X-ray reflectivity data were collected. Solid lines show when dissolved species have concentrations greater than 10^{-4} M. Dashed or dot-dashed lines indicate concentrations of ≤ 10^{-4} M.

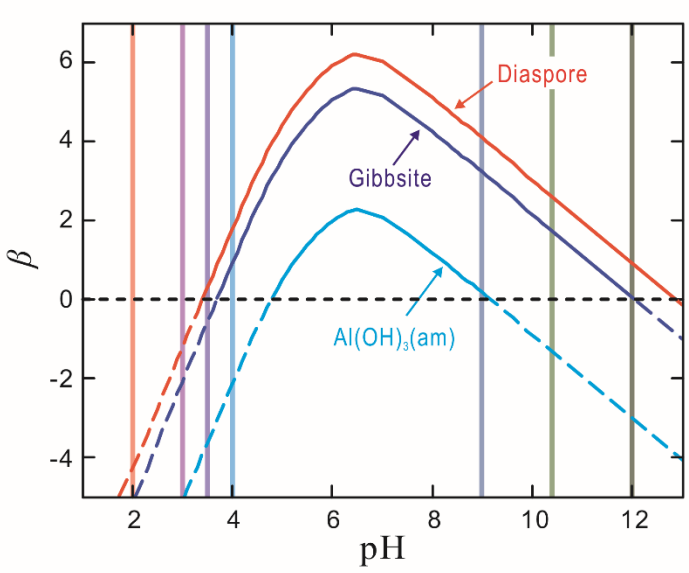

Figure 2. Saturation indices (β) of gibbsite, diaspore, and amorphous Al hydroxide ($Al(OH)_3(am)$) as a function of pH with a fixed total Al(III) content of 1 mM. Solid line segments represent supersaturation and dashed line segments represent undersaturation with respect to each solid. The vertical lines indicate the pH values where XR data were measured.

2.1.1. Growth experiments. Each muscovite crystal, having dimensions of 25 mm × 25 mm × 0.15 mm (obtained from Asheville-Shoonmaker Mica Co.), was cleaved, immediately rinsed with DIW, and transferred to a 50 mL centrifuge tube containing ~30 mL of an experimental solution. The reaction time varied depending on solution pH. Our previous study showed that a gibbsite layer formed and covered more than 50% of the muscovite (001) surface after reaction in 0.1 mM $AlCl_3$ at pH 4.2 for 18 h.[43] In 1 mM $AlCl_3$ at pH 4 (Al4), a similar film coverage was achieved in a shorter reaction time of 8 h (see Results and Discussion section for details). For the solutions that were more acidic, each sample was reacted for a longer reaction time based on the assumption that the heterogeneous nucleation rate of gibbsite on the muscovite surface is controlled by the saturation index (Fig. 2). Likewise, the reaction time was increased for the samples at more basic pH (Table 1). After reaction, the wet crystal was transferred to a closed thin-film X-ray cell[57] for *in situ* XR measurements under a capillary film of solution held in place by a 8-μm thick Kapton® film.

Table 1. Summary of Experiment Details.

samples	solution composition	reaction time (h)	beamline	energy (keV)
growth experiments				
Al2	1 mM $AlCl_3$ at pH 2	58	6-ID-B	14.00
Al3	1 mM $AlCl_3$ at pH 3	29	6-ID-B	14.00
Al3.5	1 mM $AlCl_3$ at pH 3.5	24	6-ID-B	14.00
Al4	1 mM $AlCl_3$ at pH 4	8	33-ID-D	13.05
Al9	1 mM $AlCl_3$ at pH 9	33	6-ID-B	14.00
Al10.4	1 mM $AlCl_3$ at pH 10.4	53	6-ID-B	14.00
Al12	1 mM $AlCl_3$ at pH 12	60	6-ID-B	14.00
dissolution experiments [a]				
$Al_{0.1}4.2$	(1) 0.1 mM $AlCl_3$ at pH 4.2	24	6-ID-B	14.00
Al_{DIW}	(2) DIW	30	6-ID-B	14.00
Al4[b]	(1) 1 mM $AlCl_3$ at pH 4 [b]	11		
Al_{HCl}	(2) HCl at pH 4	40	33-ID-D	13.05

[a] Sequential experiments where a freshly cleaved muscovite crystal was reacted with solution (1) to form an overgrowth and then solution (2) to dissolve the overgrowth.

[b] Prepared by reacting a freshly cleaved muscovite crystal in a solution that had the same composition as Al4 in the growth experiments but for a longer reaction time (11 h vs. 8 h). No X-ray reflectivity data were collected for this Al4 before reacting the sample with HCl solution at pH 4.

2.1.2. Dissolution experiments. The stability of gibbsite-layer films formed on the muscovite (001) surface was tested under two Al-free solution conditions. The basal surface of a freshly cleaved muscovite mica was reacted in a 0.1 mM $AlCl_3$ solution at pH 4.2 for 24 h (labelled as $Al_{0.1}4.2$), i.e., the same solution composition as those used in the previous study[43] but for a longer reaction time (i.e., 24 vs. 18 h). The reacted sample was rinsed gently with DIW and then immersed in 50 mL of DIW for 30 h. The DIW was replaced approximately every 10 h to minimize potential saturation of the solution by desorbed Al that could affect the dissolution rate. For example, desorption of the gibbsite-layer films from the muscovite could have resulted in an increase in the

total dissolved Al concentration up to 1×10^{-7} M, high enough to saturate the solution with respect to gibbsite (β = 0.8), assuming the solution pH remained constant (~5.6; the pH of water equilibrated with the atmosphere). The sample prepared by this sequential dissolution experiment is referred to as Al_{DIW} hereafter. The other sample was prepared by reacting the (001) surface of another freshly cleaved muscovite crystal with a 1 mM $AlCl_3$ solution at pH 4 for 11 h, i.e., the same solution composition as Al4 but reacted for a slightly longer time (11 h vs. 8 h). This sample was rinsed with DIW, and then the wet crystal was immersed in 50 mL of HCl solution at pH 4 for 40 h. Calculations predicted that the solution would be undersaturated with respect to gibbsite even after complete dissolution of the film (β = −3.5). The sample prepared by this second dissolution sequence is referred to as Al_{HCl} hereafter. After the reaction, each of the crystals was transferred to a thin-film X-ray cell[57] for *in situ* XR measurements.

2.2. X-ray reflectivity measurements

X-ray data were collected at beamlines 6-ID-B and 33-ID-D of the Advanced Photon Source (APS) (Table 1). At 6-ID-B, the monochromatic incident X-ray beam at 14.00 keV (i.e., wavelength, λ, of 0.886 Å) was collimated by slits of 0.3 mm (vertical, *v*) × 1.0 mm (horizontal, *h*) and focused vertically by a Kirkpatrick-Baez mirror. The focused beam had a size of 0.04 mm (*v*) × 1.0 mm (*h*) with a flux of $\sim1\times10^{12}$ photons/sec at the sample position. At 33-ID-D, the incident beam at 13.05 keV (i.e., λ of 0.950 Å) was collimated by slits to 0.2 mm (*v*) × 1.0 mm (*h*), and had a flux of $\sim5\times10^{11}$ photons/sec at the sample position.

In situ crystal truncation rod (CTR) data were collected in the specular geometry as a function of momentum transfer q, defined as $4\pi\sin(2\theta/2)/\lambda = 2\pi L/d$, where 2θ is the angle between the incident and reflected X-rays, L is the Bragg index of the muscovite (001) reflection, and d = ~19.96 Å is the (001) layer spacing.[52] Each dataset was collected in the q range from ~0.16 to 5.32

$Å^{-1}$. During data collection, the sample was periodically translated within the scattering plane to minimize changes in the gibbsite film structure by X-rays.[43] The translation distance was short (± 0.4 mm, overall) so that the whole reflectivity dataset could be collected within the area illuminated by X-rays at the lowest angle, but long enough to ensure that X-rays could illuminate a new spot when the sample was translated at higher angles.

2.3. Data analyses

The CTR data were fit to a structural model consisting of solid muscovite, the interfacial solution near the muscovite (001) surface, and the bulk solution above this interfacial region. The bulk muscovite structure was modeled based on single crystal X-ray diffraction results for crystals from the same source.[52] All atoms in bulk muscovite were fixed at their crystallographic positions except those in the top two unit-cell layers of the surface (i.e., up to about 40 Å depth from the muscovite surface). The atoms in these layers were allowed to relax along the surface normal direction, to which the specular CTR is sensitive. The model for the interfacial solution included adsorbed species, water molecules, and gibbsite-layer films. The electron-density distribution of each atomic/molecular layer (or plane) projected on the axis perpendicular to the muscovite surface was modelled using a Gaussian peak defined by the occupancy (o), height from the top oxygen plane of the muscovite surface (z), and root-mean-square (rms) distribution width (u) (Tables S3–12).[43] The bulk solution structure above the interfacial region was expressed with the *layered water model*.[58]

X-ray reflectivity, R, defined as the ratio of the reflected to incident X-ray intensities, was calculated as

$$R \propto (4\pi r_e/qA_{UC})^2 \mid F_{UC} F_{CTR} + F_{INT} + F_W \mid^2 \qquad (4)$$

where $r_e = 2.818 \times 10^{-5}$ Å is the electron radius and $A_{UC} = 46.72$ Å^2 is the area of the unit cell on the muscovite (001) plane. F_{UC}, F_{INT}, and F_W are the structure factors of a muscovite unit cell, interfacial region, and fluid water, respectively, and F_{CTR} is the CTR form factor and calculated as $1/[1-\exp(-iqd/2)]$ where d is the (001) spacing of the muscovite (~19.96 Å).[52] The structure factor of a given sub-layer ℓ was calculated as

$$F_\ell = \Sigma_j o_j f_j(q) \exp(iqz_j) \exp[-(qu_j)^2/2] \quad (5)$$

where $f_j(q)$ is the atomic scattering factor.[59]

Various models were tested by changing the number of peaks (from 3 to 8) for each data set, and the best-fit model was chosen based on the smallest χ^2 defined as

$$\chi^2 = [\Sigma_k (I_k - I_{calc,k})^2/\sigma_k^2]/(N - N_p) \quad (6)$$

where N and N_p are the numbers of data points and parameters used in the model fit, respectively, I_k and $I_{calc,k}$ are the measured and calculated intensities, respectively, and σ_k is the uncertainty of the k^{th} data point. The covariance among fitting parameters[60] was also considered and minimized to determine the optimal number of model parameters. The R-factor ($\Sigma_k |(I_k - I_{calc,k})/I_k|/N$) of the best-fit is also reported for comparison.

The interfacial electron-density profile derived from the best-fit model is plotted as a function of height (z) from the surface. The origin, $z = 0$, is chosen at the average height of the oxygen atoms in the basal surface plane of muscovite. All electron-density profiles shown in this study are broadened by the experimental resolution (π/q_{max}),[61] and normalized to that of bulk water (~0.33 $e^-/Å^3$).

3. Results and Discussion

3.1. Muscovite (001)–$AlCl_3$ solution interface at acidic pH

Specular CTR data of the muscovite (001)–$AlCl_3$ solution interface show significant differences over the pH range of 2 to 4. The large intensity variations dominated by Bragg reflections of the bulk muscovite crystal (Fig. S1) were normalized to the generic CTR shape $(1/[q\sin(qd/4)^2])$[57] to enhance the visibility of smaller intensity variations due to changes in interfacial structures. At pH 4 (where the saturation index (β) for gibbsite is 0.91, Table S2), the normalized CTR data show a clear oscillatory feature over the entire q range. This oscillatory feature is similar to that observed previously in 0.1 mM $AlCl_3$ at pH 4.2 (β = ~0.7), where the formation of a well-defined gibbsite-layer film was observed at the muscovite (001)–solution interface.[43] This oscillation is less pronounced for Al3.5, indicating either lower coverage or more disordered structure of the film compared with Al4. The CTR data for Al3 are similar to those for Al3.5, indicating that the interfacial structures were comparable at these two pH values. In contrast, the CTR data for Al2 are considerably different from the Al3 and Al3.5 data, especially for $q < 2$ Å^{-1}. For example, a factor of five decrease in intensity was observed at q = 1.5 Å^{-1} from Al3 to Al2. Instead, the Al2 data look similar to those measured in DIW or pH 2.5 HCl solution without Al (corresponding to dashed black and dotted blue curves, respectively, in Fig. 3) while they significantly deviate from the DIW data at $q \geq$ ~3.8 Å^{-1}.[58,62] Because these CTR data are sensitive to the electron density distribution at the muscovite–solution surface, the similarity between the Al2 and pH 2.5 HCl data indicates that the solution structures near the muscovite surface for these two solutions are likely also similar.

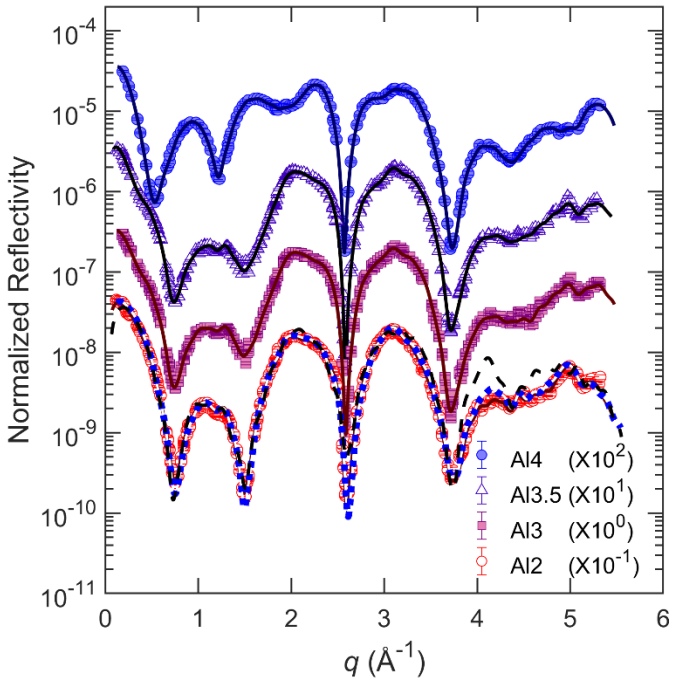

Figure 3. Normalized *in situ* specular CTR data at the muscovite (001)–1 mM $AlCl_3$ solution interface at pH 2, 3, 3.5, and 4. The solid lines through the data points were calculated from the best-fit models. The datasets were scaled vertically for clarity using the multiplicative factors given in parentheses after the sample names. The Al2 data are compared with the normalized reflectivity data calculated from the best-fit models for the muscovite (001) in contact with deionized water (DIW)[58] and pH 2.5 HCl solution[62] shown in dashed (black) and dotted (blue) lines, respectively.

The CTR data were analyzed using structural models to yield the total electron-density profiles at the muscovite (001)–$AlCl_3$ solution interface as a function of pH. The derived profiles show the electron density distribution projected on the axis perpendicular to the muscovite (001) surface. At pH 2, the best-fit model profile (χ^2 = 2.53, Table S3) has three broad electron-density peaks at heights around 2.7, 6.5, and 9.8 Å from the muscovite surface. The first peak at 2.7 Å is broad, (i.e., rms width of ~1.0 Å) and has an electron density significantly higher than that of bulk water. The maximum electron density of this peak is about twice as high as the bulk water density (Fig. 4). In contrast, the other two peaks have electron densities similar to the bulk water density. The

solution profile at larger distances from the surface is mostly featureless. The best-fit model also has a small electron-density peak at ~0.3 Å, which is hard to distinguish visually because it overlaps the electron density of the top oxygen plane of the muscovite surface (Fig. 4). A model without this yielded a ~16% higher χ^2 value (i.e., less good agreement between the data and calculation; result not shown), indicating its small but significant contribution to the quality of fit of the model structure to the experimental data. Overall, the derived electron-density profile is similar to that observed in HCl solution without Al at pH 2.5 but somewhat different from that in DIW.[58,62] The electron-density profile in DIW has two distinct electron-density peaks at 1.3 and 2.5 Å from the muscovite surface (Fig. 4), which are consistent with the heights of water molecules that adsorb in ditrigonal cavities and on the top of the surface oxygen plane, respectively.[58] These adsorbed water molecules define the first hydration layer of the muscovite surface with the coverage of ~2.3 H_2O/A_{UC}.[58] In contrast, the solution profile near the muscovite surface for Al2 has one broad electron-density peak. This difference can result from adsorption of (hydrated) Al(III) as well as hydronium whose difference in adsorption height and coverage cannot be determined with the experimental resolution (~0.6 Å in z).

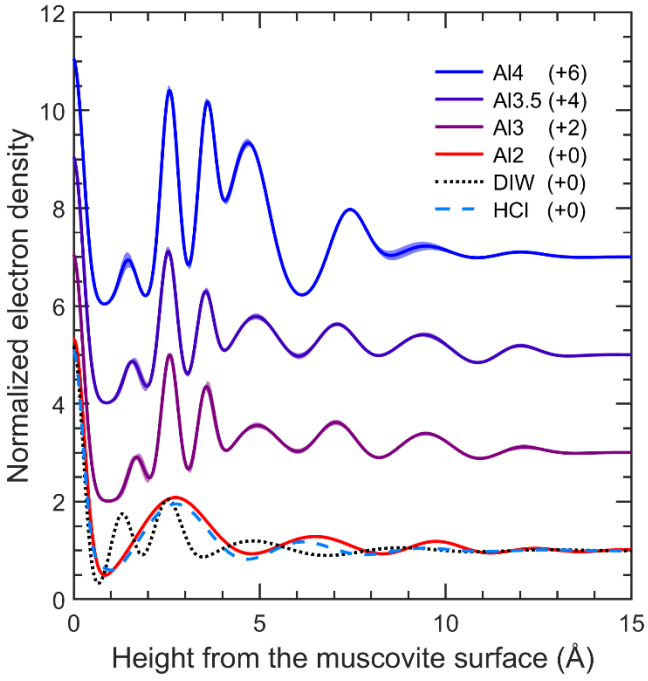

Figure 4. Electron-density profiles at the muscovite (001)–1 mM $AlCl_3$ solution interface at pH 2, 3, 3.5, and 4. The profiles for the muscovite (001)–deionized water (DIW) interface[58] and muscovite (001)–HCl solution interface at pH 2.52[62] are also shown for comparison. The datasets are offset vertically for clarity as indicated by the number in the parentheses after each sample name in the legend.

The electron-density profiles measured at pH 3, 3.5, and 4 (Al3, Al3.5, and Al4, respectively) are significantly different from that at pH 2. The best-fit model profiles for Al3 and Al3.5 (χ^2 = 3.17 and 3.33, respectively; Tables S4 and 5) have four distinct electron-density peaks: one small electron-density peak at ~1.6 Å, two more-electron-dense peaks at ~2.6 and ~3.5 Å, and a broad peak at ~4.9 Å (Fig. 4). This structure is followed by an oscillatory feature whose magnitude decreases with distance from the surface. The electron-density profile derived from the best-fit model for Al4 (χ^2 = 1.13; Table S6) also has distinct electron-density peaks that are located at heights similar to those for Al3 and Al3.5. The smallest peak at 1.5 Å has a comparable electron density to those observed at similar heights in the Al3 and Al3.5 profiles. In contrast, three electron-density peaks in Al4 located within 2–6 Å in height have significantly higher intensities than those located in the same range for Al3 and Al3.5 (Fig. 4). This three-peak layer structure is

similar to that of a single-layer gibbsite film formed at the muscovite surface after reaction in 0.1 mM $AlCl_3$ at pH 4.2 for 18 h.[43] The Al4 profile also has a broad electron-density peak at 7.4 Å, with a higher electron density than that of bulk water (Fig. 4). Together with a peak at 9.4 Å, it has a layer thickness that matches the thickness of a gibbsite layer (Fig. S2). Based on these observations, this layer is interpreted to contain a second gibbsite layer. However, the intramolecular planes within this presumed second gibbsite layer are less distinct compared with the first layer, indicating that the structure is likely more disordered with respect to the muscovite (001) plane. The total integrated electron density of this second layer is also lower than the first layer (Table S6), indicating its smaller surface coverage.

The areal coverages of the gibbsite-layer films were estimated based on the difference of the interfacial electron density above the muscovite surface from that of DIW. At pH 4, the solution layer including the first gibbsite layer, i.e., up to z = ~6 Å, has an integrated electron density that is almost twice as high as that of bulk water. This integrated electron density equates to ~85% areal coverage of the gibbsite-layer film, indicating incomplete film coverage. The film-free surface was likely covered with the hydration layer, which was ignored in this calculation. A calculation based on the more realistic assumption that the surface was covered by either water or gibbsite-layer film yields ~70% areal coverage of the film. The electron density above this gibbsite layer is also slightly higher than the bulk water density, presumably due to the partial coverage of bilayer gibbsite. The areal coverage of this second gibbsite layer is estimated to be ~15%. The Al3 and Al3.5 profiles also have similar electron-density patterns, indicating the presence of the gibbsite-layer films. However, these films are less distinct and lower in electron density, having estimated areal coverages of the first gibbsite layer of ~20%, which is about 1/4 of the coverage for Al4. These smaller coverages can indicate that the film formation was either significantly slower or saturated at a lower coverage at pH 3 and 3.5 than pH 4. No evidence for the formation of a gibbsite-layer film was observed for Al2.

3.2. Muscovite (001)–$AlCl_3$ interface at basic pH

The CTR data measured at three basic pH conditions are all similar to those measured in DIW,[58] except for small differences at $2 \leq q \leq 2.5$ Å^{-1} and $q \geq 3.8$ Å^{-1} (Fig. 5). The best-fit model profiles for all three samples have two electron-density peaks at 1.8 and 3.0 Å, which partially overlap each other, followed by a broad peak distributed between 4 and 8 Å (Fig. 6). Overall, these features are generally similar to those in DIW although they are located slightly farther (by ~0.5 Å) from the surface than in DIW (Fig. 6). It is inferred that these small changes result from adsorption of cations to the muscovite surface, including Na^+, as the solutions contained up to 10 mM Na. The amount of adsorbed Na^+ was not quantified because it is difficult to distinguish from adsorbed water molecules by CTR. No gibbsite-layer film structure was observed in the basic $AlCl_3$ solutions in stark contrast to the data measured in Al3, Al3.5, and Al4.

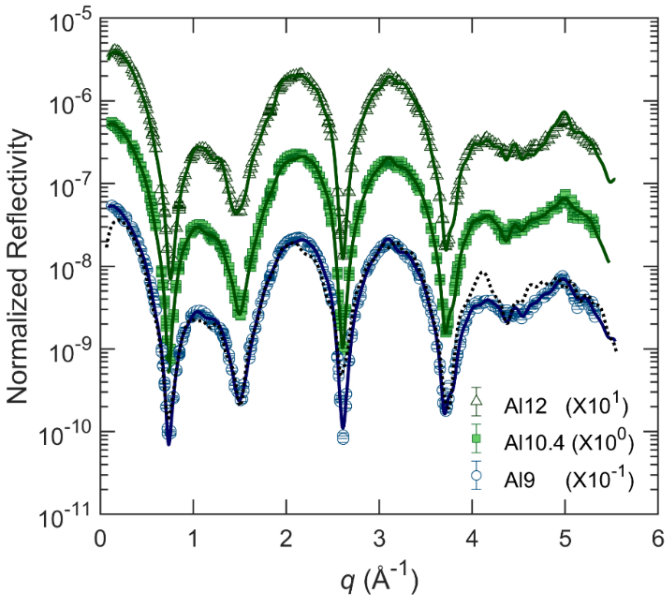

Figure 5. Normalized *in situ* specular CTR data at the muscovite (001)–1 mM $AlCl_3$ solution interface at pH 9, 10.4, and 12. The solid lines through the data points were calculated from the best-fit models. The normalized reflectivity calculated from the best-fit model of the CTR data for the muscovite (001)–DIW interface[58] is shown as a short-dashed line with the Al9 data for comparison. The datasets were scaled vertically for clarity using the factors shown in the parentheses after the sample names.

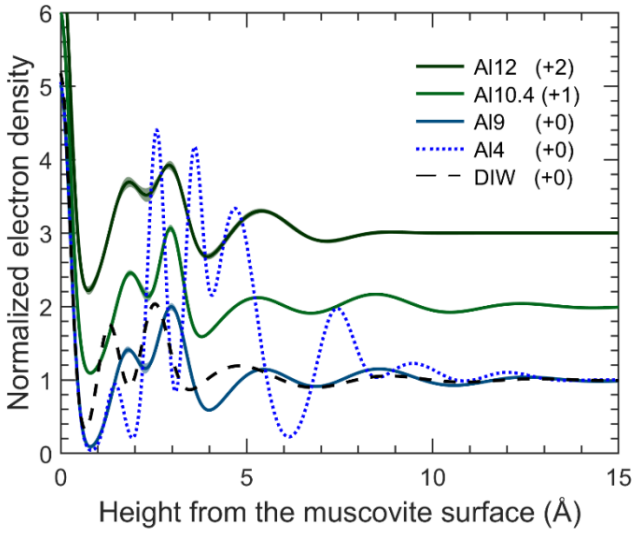

Figure 6. Electron-density profiles at the muscovite–1 mM $AlCl_3$ solution interface at pH 9, 10.4, and 12. The profile for the $AlCl_3$ data at pH 4 and that for the muscovite (001)–DIW interface[58] are also shown for comparison. The datasets are offset vertically, as indicated by the number in the parentheses after each sample name in the legend, for clarity.

3.3. Effect of pH on nucleation of gibbsite-layer films on muscovite

The derived electron-density profiles for Al3, Al3.5, and Al4 show clear evidence of the formation of gibbsite-layer films on the muscovite (001) surface. The highest coverage gibbsite film was observed at pH 4, where the solution was slightly supersaturated with respect to gibbsite. Similar gibbsite-layer films were observed at pH 3 and 3.5, but with lower film coverages than that at pH 4. The samples at pH 3 and 3.5 were reacted for longer times than that at pH 4 (i.e., 29 and 24 h for Al3 and Al3.5 vs. 8 h for Al4; Table 1), indicating that solution pH, that determines the saturation state of gibbsite, has a larger influence on the film coverage than reaction time. These solutions were undersaturated with respect to gibbsite (Fig. 2 and Table S2). The growth of gibbsite-layer films from solutions undersaturated with respect to gibbsite (i.e., Al3 and Al3.5) demonstrates the influence of the muscovite surface in the nucleation and growth of this secondary phase at acidic pH.

The surface-promoted nucleation and growth of gibbsite on muscovite (001) in mildly acidic solutions can be explained by a stepwise reaction as described schematically in Figure 7. In these solutions, Al(III) exists mostly as positively charged species, i.e., Al^{3+} and $AlOH^{2+}$ (Fig.1 and Table S1), which can adsorb on the negatively charged muscovite surface by electrostatic attraction (Fig. 7a). Previous studies of adsorption of cations on the muscovite surface revealed the coexistence of multiple adsorbed species, including partially hydrated inner-sphere (IS) and fully hydrated outer-sphere (OS) surface complexes.[63] The fractional coverages of these species strongly depend on the charge and hydration free energy of cations. For example, adsorption of Al^{3+} on the muscovite surface may be comparable to that of Y^{3+}, which adsorbs predominantly as OS complexes that are distributed within 10 Å from the muscovite surface.[64] These OS complexes are presumably more mobile at the interface than IS complexes that are observed to occupy the ditrigonal cavities of the surface. The local concentration of Al^{3+} near the surface can be as high as ~1 M for a cation coverage that is high enough to compensate fully the structural charge of muscovite ($1e^-/A_{UC}$, or 0.33 Al^{3+}/A_{UC}). An even higher local concentration, ~1.5 M, can be obtained upon adsorption of divalent $AlOH^{2+}$ that exists as a minor species in the solutions (Fig. 7b). In contrast, the dominant Al(III) species at basic pH is anionic $Al(OH)_4^-$, which is likely excluded by electrostatic repulsion from the negatively-charged muscovite surface. Therefore, it appears that adsorption of Al(III) at the interface is the main driving force for the formation of the gibbsite-layer film at the interface in mildly acidic conditions.

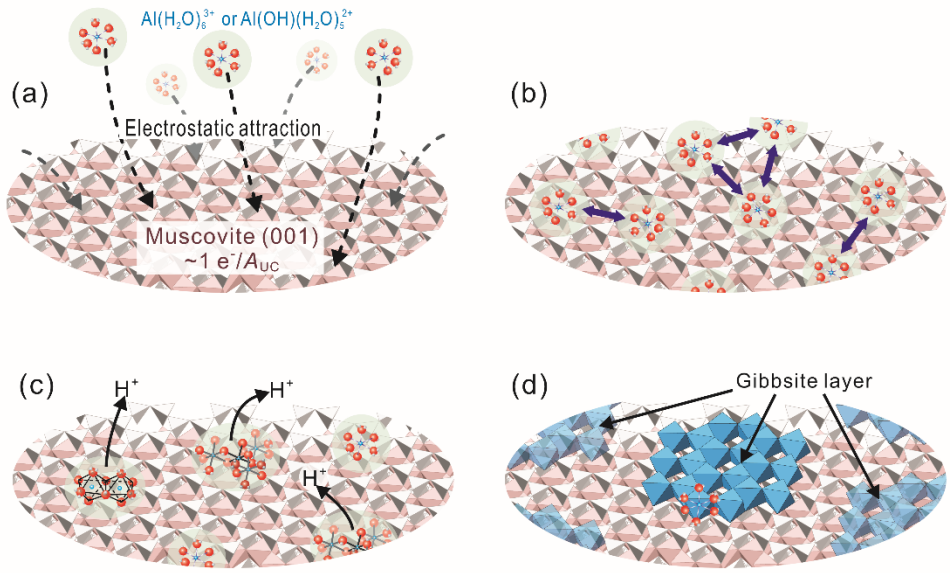

Figure 7. Proposed sequence of the gibbsite-layer film formation on the muscovite (001) surface. **(a)** Hydrated Al(III) species, e.g., $Al(H_2O)_6^{3+}$ or $Al(OH)(H_2O)_5^{2+}$, adsorb on the negatively-charged surface by electrostatic attraction. **(b)** These Al species likely adsorb as outer-sphere complexes, having a relatively high mobility at the interface. **(c)** Reactions between the adsorbates can yield the formation of oligomeric species that can act as intermediate-state pre-nuclei for gibbsite-layer films. **(d)** Lateral extension of the polymerization process results in the formation of patched gibbsite-layer films.

We propose that the increased local concentration and expected high mobility of Al(III) species adsorbed at the interface can lead to the formation of Al oligomers (Fig. 7c). For example, Al hydroxo dimers can form by olation[65-66] as

$$2Al(H_2O)_6^{3+} \rightarrow [(H_2O)_5Al-OH-Al(H_2O)_5]^{5+} + H_2O + H^+ \quad (7)$$

$$\rightarrow [(H_2O)_4Al\langle^{OH}_{OH}\rangle Al(H_2O)_4]^{4+} + 2H_2O + 2H^+ \quad (8)$$

These processes produce protons, indicating that the solution near the surface can become more acidic than the bulk solution (Fig. 7c). At the same time, the effective positive charge of each Al(III) decreases, e.g., from 3 to 2.5 to 2 by the reactions (Eqs. 6 and 7), which, potentially, leads to additional adsorption of cationic Al species from the solution to the muscovite surface. This inferred enhancement of the Al(III) coverage *beyond* the amount needed for the surface charge

compensation can be an additional driving force for the spontaneous formation of gibbsite-layer films at the interface (Fig. 7d).

3.4. Structural relationship between muscovite mica and gibbsite-layer film

The gibbsite layer nucleated at mildly acidic pH grew into a mono-molecular-thick film, indicating that the polymerization occurred exclusively along the surface. Although our current X-ray data do not show the reaction pathway from adsorbed monomeric Al species to the 2D film, possible mechanisms for the transformation can be suggested. For example, the progression of olation (Eq. 7) between adsorbed Al species can lead to the formation of oligomers whose structure resembles the structure of a gibbsite layer. The simplest form of these oligomers includes an Al tetramer, $[Al_4(OH)_{8+x}(H_2O)_{12-x}]^{4-x}$, where the central Al is double-hydroxo-bonded to three hydrated Al ions, or an Al hexamer, $[Al_6(OH)_{12+x}(H_2O)_{12-x}]^{6-x}$, where double-hydroxo-bonded Al ions form a six-membered ring structure.[28,45] These oligomers can act as nucleation sites for the 2D propagation of polymerization reactions along the basal plane of muscovite. Depending on their stability, these species can also behave as prenucleation clusters, consistent with those proposed in a non-classical crystal growth pathway,[67-68] whose aggregation, presumably via olation, along the basal surface of muscovite results in the formation of the film at the interface.

The specular CTR analyses showed incomplete coverages of the gibbsite-layer films, indicating that the two-dimensional growth was limited in its lateral expansion. This interpretation is consistent with a previous AFM observation that the gibbsite-layer films were composed exclusively of about 10 to 20 nm wide and ≤1 nm high *islands* after reactions in 0.1 mM Al(III) at pH 4.2 for up to 50 h.[43] An *ex situ* CTR dataset measured after reaction in the solution with this composition showed that the areal coverage of the films was unchanged over 3000 h. The limited lateral expansion of the gibbsite nanoparticles can be explained partly by the slight mismatch of the lattice constants between muscovite and gibbsite. The area of the unit cell on the basal surface of gibbsite is about 6% smaller than that of muscovite,[52] and therefore the epitaxial film growth,

if present, requires a lateral expansion, i.e., tensile strain, of the film lattice. For our study of the gibbsite-layer film on the muscovite (001) surface, the specular CTR data probe only the structural ordering along the surface normal direction with limited sensitivity to the lateral position of the film with respect to the underlying surface. Additional measurements, such as 3D CTR measurements in both specular and non-specular geometries as well as *in situ* AFM, could be applied to provide direct insight into the lateral epitaxial relationship at the muscovite (001)–gibbsite-layer film interface.

3.5. Stability of Al (oxy)hydroxide films on muscovite (001)

The inferred strain in the gibbsite films resulting from the epitaxy with the muscovite substrate imply that these thin layers of gibbsite may have a different thermodynamic stability from bulk gibbsite. We conducted dissolution experiments to test the relative stability of the films. The stability was measured by reacting each of two pre-grown films in either DIW at pH 5.6 for 30 h or dilute HCl at pH 4 for 40 h. The samples after these dissolution experiments were labelled as Al_{DIW} and Al_{HCl}, respectively. The results showed a clear difference in the stability of the gibbsite films in the two solutions. The CTR data from the Al_{DIW} experiment are similar to those collected before the reaction, indicating that the gibbsite-layer film on the muscovite surface was mostly unchanged. In contrast, the data from the Al_{HCl} experiment are significantly different (Fig. 8), indicating nearly complete dissolution of the gibbsite film.

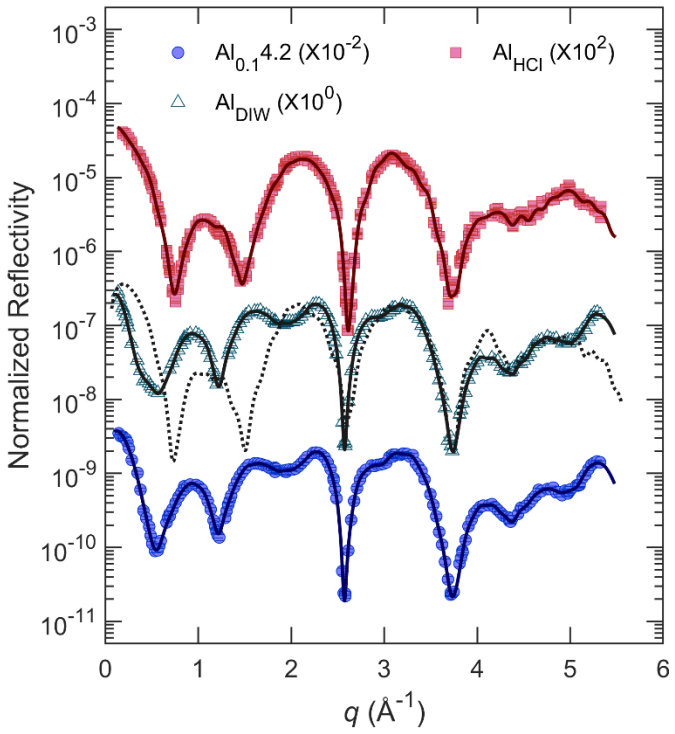

Figure 8. Normalized X-ray reflectivity at the muscovite–$AlCl_3$ solution interface during the sequential dissolution experiment. The data from the muscovite with the gibbsite-layer film pregrown in 0.1 mM Al ($Al_{0.1}4.2$), and the film after reaction with DIW for 30 h (Al_{DIW}) and pH 4 HCl solution for 40 h (Al_{HCl}) are shown in blue circles, green triangles, and red squares, respectively. The solid lines through the data points are calculated from the best-fit models (Tables S10–12). The normalized X-ray reflectivity calculated from the best-fit model for the muscovite (001)–DIW interface[58] (short-dashed line) is also shown with the Al_{DIW} data for comparison. The datasets are offset vertically for clarity as indicated.

The derived electron-density profile after reaction in DIW (Al_{DIW}) is similar to that obtained before the reaction (Fig. 9). The best-fit model profile maintains three sharp peaks, indicative of the first layer of the gibbsite film, located at similar heights (Tables S10 and 11). The second layer of gibbsite, located in the height range from 6 to 11 Å, shows small changes: the peak at ~6.5 Å became more electron dense and the peak at 9.5 Å became broader. In addition, the profile has a decreased coverage for the species adsorbed at ~1.4 Å. Larger changes were observed in the electron-density profile after reaction in the pH 4 HCl solution (Al_{HCl}). The derived profile for

Al_{HCl} has no well-defined gibbsite-layer films at the surface, indicating almost complete dissociation of the gibbsite-layer film (Fig. 9). Rather, the profile is similar to that observed previously in the pH 2.5 HCl solution without Al[62] (Fig. 4). In the Al_{HCl} experiment, hydronium can adsorb and compensate negative charge on the muscovite surface that is exposed after dissolution of the gibbsite-layer film. At this condition, the bulk hydronium concentration is calculated to be at least three orders of magnitude higher than the Al(III) concentration if the gibbsite layer was completely dissolved. Using these concentrations, we estimate that the coverage of hydronium can be as high as 90% (where 100% is the cation coverage needed for the full compensation of the surface charge) when calculated using the intrinsic adsorption constant of hydronium against that of Y^{3+} as an analogue for Al^{3+}.[64,69]

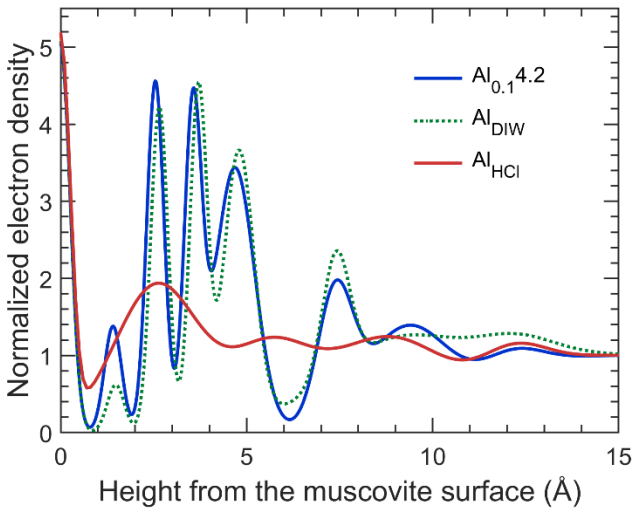

Figure 9. Electron-density profiles at the muscovite–$AlCl_3$ solution interface during the dissolution experiment. The best-fit model profiles for the muscovite with the gibbsite-layer film pregrown in 0.1 mM Al at pH 4.2 ($Al_{0.1}$4.2), and the film after reaction with DIW for 30 h (Al_{DIW}) and pH 4 HCl solution for 40 h (Al_{HCl}) are shown in blue solid, green dotted, and red solid lines, respectively.

The different structural evolution of the gibbsite layer films in the two Al-free solutions indicates that solution pH is a critical factor for determining the film stability at the muscovite–solution interface. For bulk crystalline gibbsite, acidic dissolution occurs mainly by the protonation of hydroxyl groups followed by the cleavage of the hydroxide bonds between two adjacent Al ions via dehydration.[5,70] Therefore, it is expected that the reaction rate would increase rapidly with increasing proton (or hydronium) concentration. The HCl solution also contained Cl^-, but the effect of this anion on gibbsite film dissolution was likely negligible because of its low concentration (10^{-4} M) in the experimental solution.

While the stability of the film was expected in DIW (pH ~5.6), the complete dissolution of the gibbsite-layer films after 40 h of reaction in the pH 4 HCl solution was unexpected when compared with the dissolution rate of bulk gibbsite. For example, the dissolution rate of bulk gibbsite normalized to the surface area is as low as 10^{-12} mol m^{-2} sec^{-1} or ~4×10^{-9} mol m^{-2} h^{-1} in pH 4 HCl.[70] Conversion of this value to the dissolution rate for Al(III) per area of the unit cell of gibbsite (001) ($A_{UC,gibbsite}$ = ~44.1 $Å^2$) is ~2×10^{-4} Al $A_{UC,gibbsite}^{-1}$ h^{-1}. This suggests that the dissolution of single-layer gibbsite should take ~150 d in the pH 4 solution, approximately two orders of magnitude longer than the reaction period applied in our study (40 h = ~1.7 d). We propose that the enhanced dissolution rate of the gibbsite-layer film can be interpreted to be a result of the internal tensile strain of the films associated with the 6% mismatch with the unit cell area of the muscovite (001) surface. Overall, this comparison indicates that the gibbsite-layer films that are formed on the muscovite surface are less stable than bulk gibbsite in acidic conditions.

4. Conclusions

The results show that gibbsite-layer films can form on the muscovite mica surface at mildly acidic pH solutions that are saturated or even slightly undersaturated with respect to gibbsite.

Similar conditions can exist in nature where high concentrations of Al, up to the millimolar, are induced by dissolution of Al-containing silicate minerals in acidified soils and sediments.[71] Thin films of gibbsite can form on the muscovite surface even from a solution undersaturated with respect to gibbsite. Similar reactions may occur on the basal surfaces of many clay minerals, which also possess both the negative charge that can attract dissolved Al and the (quasi-)hexagonal lattice structure that can facilitate the formation of epitaxial gibbsite layers. Depending on the solution composition and pH, the film may incorporate trace cationic species, e.g., as observed from our previous X-ray experiments on the incorporation of Ga in the film structure,[43] or may form different mineral phases, e.g., layered double hydroxides.[72] Because film formation involves adsorption and accumulation of Al(III) at the interface, it can occur at conditions with even lower dissolved Al contents through the additional stabilization of electrostatic attraction of Al species to a mineral surface.

The formation of gibbsite-layer films should also affect the reactivity of the underlying minerals. Muscovite and many clay minerals have a negative structural charge, on which ion adsorption is largely driven by short-range electrostatic interaction (e.g., formation of the Stern layer). The gibbsite-layer film can physically block the surface adsorption sites, hampering the direct interaction between these surface sites and cationic solutes. This can alter the adsorption mode and strength, and thereby the chemical stability of adsorbates at the interface. The gibbsite-layer films can also produce new adsorption sites at the interface. In particular, gibbsite, along with other Al (oxy)hydroxide phases, is known to be a strong sorbent for anions.[13-14] The positive charge of gibbsite can originate from the protonation of surface hydroxyl groups. This protonation has been assumed to occur mostly at singly coordinated Al sites, ≡Al–OH, that exist only on the edges of the crystal, with pK_a of ~10.[17,73] In contrast, the doubly-coordinated Al sites on the basal plane have been assumed to be proton inactive.[74] The pH-dependent variation of the charge of the

basal surface of gibbsite was investigated by an AFM colloidal probe technique in NaCl solution.[75] The results revealed a single pK_a value of 5.9 ± 0.2 for the hydroxyl groups at the basal surface. However, the saturated surface potential below the pK_a was only 12 mV by zeta-potential measurements, indicating that only a small fraction of the surface functional groups is proton active. From this result, the maximum diffuse layer charge density calculated using the Gouy-Chapman theory was only 0.0008 C/m^2, i.e., less than 1% of the surface charge of muscovite (~0.32 C/m^2). Therefore, additional sorption of ions can occur likely at the edge sites of the gibbsite layer nuclei or within the layer, e.g., by either isomorphic substitution[43] or incorporation, during the film formation.

As a sorbent, the gibbsite-layer films appear to be less effective for long-term sequestration of sorbate elements. Dissolution experiments indicate that the gibbsite-layer films formed on the muscovite surface are significantly less stable than bulk gibbsite at acidic pH. Therefore, such films can be described as metastable, with a stability that can be influenced by changes in solution acidity and composition. Relatively fast reaction dynamics between formation (which sequesters Al and other elements that are sorbed on and associated in the film) and dissolution (which releases the captured elements to natural waters) indicates that these and similar films can play a key role in controlling short-term variations of the composition of pore water or groundwater in many mica- or clay-rich rock and soil environments.

Associated Content

Supporting Information

The Supporting Information is available free of charge on the ACS Publication website.

Thermodynamic calculations of Al speciation and ionic strength of the solutions in growth experiments, Solid saturation indices of the solutions in growth experiments, Fitting

parameters for X-ray reflectivity data, X-ray reflectivity data at the muscovite (001)–1 mM $AlCl_3$ solution interface during film growth and dissolution experiments, Total electron-density profile for Al4.

Acknowledgment

This work was supported by U.S. Department of Energy, Office of Science, Office of Basic Energy Sciences, Chemical Sciences, Geosciences, and Biosciences Division under Contracts DE-AC02-06CH11357 to UChicago Argonne, LLC as operator of Argonne National Laboratory. M.S. has received funding from the Helmholtz Gemeinschaft Deutscher Forschungszentren by supporting the Helmholtz–Nachwuchsgruppe "Structures and Reactivity at the Water/Mineral Interface" (VH–NG–942). The X-ray data were collected at beamlines 6-ID-B and 33-ID-D, Advanced Photon Source. Use of the Advanced Photon Source was supported by the U.S. Department of Energy, Office of Science, Office of Basic Energy Sciences, under Contract DE-AC02-06CH11357 to UChicago Argonne, LLC as operator of Argonne National Laboratory. The submitted manuscript has been created by UChicago Argonne, LLC, Operator of Argonne National Laboratory ("Argonne"). Argonne, a U.S. Department of Energy Office of Science laboratory, is operated under Contract No. DE-AC02-06CH11357. The U.S. Government retains for itself, and others acting on its behalf, a paid-up nonexclusive, irrevocable worldwide license in said article to reproduce, prepare derivative works, distribute copies to the public, and perform publicly and display publicly, by or on behalf of the Government.

References

1. Browne, B. A.; Driscoll, C. T., Soluble aluminum silicates - stoichiometry, stability, and implications for environmental geochemistry. *Science* **1992,** *256*, 1667-1670.
2. Palmer, D. A.; Wesolowski, D. J., Aluminum speciation and equilibria in aqueous solution: II. The solubility of gibbsite in acidic sodium chloride solutions from 30 to 70°C. *Geochim. Cosmochim. Acta* **1992,** *56*, 1093-1111.

3. Scholl, M. A.; Harvey, R. W., Laboratory investigations on the role of sediment surface and groundwater chemistry in transport of bacteria through a contaminated sandy aquifer. *Environ. Sci. Technol.* **1992,** *26*, 1410-1417.

4. Wesolowski, D. J., Aluminum speciation and equilibria in aqueous solution: I. The solubility of gibbsite in the system Na-K-Cl-OH-$Al(OH)_4$ from 0 to 100ºC. *Geochim. Cosmochim. Acta* **1992,** *56*, 1065-1091.

5. Langmuir, D., *Aqueous Environmental Geochemistry*. Prentice-Hall, Inc.: Upper Saddle River, NJ, 1997; p 600.

6. Shock, E. L.; Sassani, D. C.; Willis, M.; Sverjensky, D. A., Inorganic species in geologic fluids: Correlations among standard molal thermodynamic properties of aqueous ions and hydroxide complexes. *Geochim. Cosmochim. Acta* **1997,** *61*, 907-950.

7. Price, J. R.; Velbel, M. A., Chemical weathering indices applied to weathering profiles developed on heterogeneous felsic metamorphic parent rocks. *Chem. Geol.* **2003,** *202*, 397-416.

8. Palmer, D. A.; Wesolowski, D. J., Aluminum speciation and equilibria in aqueous solution: III. Potentiometric determination of the first hydrolysis constant of aluminum(III) in sodium chloride solutions to 125°C. *Geochim. Cosmochim. Acta* **1993,** *57*, 2929-2938.

9. Wesolowski, D. J.; Palmer, D. A., Aluminum speciation and equilibria in aqueous solution: V. Gibbsite solubility at 50°C and pH 3-9 in 0.1 molal NaCl solutions (a general-model for aluminum speciation; analytical methods). *Geochim. Cosmochim. Acta* **1994,** *58*, 2947-2969.

10. Casey, W. H., Large aqueous aluminum hydroxide molecules. *Chem. Rev.* **2006,** *106*, 1-16.

11. Casey, W. H.; Rustad, J. R., Reaction dynamics, molecular clusters, and aqueous geochemistry. *Annu. Rev. Earth Planet. Sci.* **2007,** *35*, 21-46.

12. Rustad, J. R.; Casey, W. H., Metastable structures and isotope exchange reactions in polyoxometalate ions provide a molecular view of oxide dissolution. *Nat. Mater.* **2012,** *11*, 223-226.

13. Van Emmerik, T. J.; Sandström, D. E.; Antzutkin, O. N.; Angove, M. J.; Johnson, B. B., ^{31}P solid-state nuclear magnetic resonance study of the sorption of phosphate onto gibbsite and kaolinite. *Langmuir* **2007,** *23*, 3205-3213.

14. Huang, X.; Foster, G. D.; Honeychuck, R. V.; Schreifels, J. A., The maximum of phosphate adsorption at pH 4.0: Why it appears on aluminum oxides but not on iron oxides. *Langmuir* **2009,** *25*, 4450-4461.

15. Li, W.; Feng, X.; Yan, Y.; Sparks, D. L.; Phillips, B. L., Solid-state NMR spectroscopic study of phosphate sorption mechanisms on aluminum (hydr)oxides. *Environ. Sci. Technol.* **2013,** *47*, 8308-8315.

16. Papelis, C.; Brown, G. E., Jr.; Parks, G. A.; Leckie, J. O., X-ray absorption spectroscopic studies of cadmium and selenite adsorption on aluminum oxides. *Langmuir* **1995,** *11*, 2041-2048.

17. Hiemstra, T.; Yong, H.; Van Riemsdijk, W. H., Interfacial charging phenomena of aluminum (hydr)oxides. *Langmuir* **1999,** *15*, 5942-5955.

18. Gimsing, A. L.; Borggaard, O. K.; Sestoft, P., Modeling the kinetics of the competitive adsorption and desorption of glyphosate and phosphate on goethite and gibbsite and in soils. *Environ. Sci. Technol.* **2004,** *38*, 1718-1722.

19. Duarte, G.; Ciminelli, V. S. T.; Dantas, M. S. S.; Duarte, H. A.; Vasconcelos, I. F.; Oliveira, A. F.; Osseo-Asare, K., As(III) immobilization on gibbsite: Investigation of the complexation mechanism by combining EXAFS analyses and DFT calculations. *Geochim. Cosmochim. Acta* **2012,** *83*, 205-216.

20. Goldberg, S., Macroscopic experimental and modeling evaluation of selenite and selenate adsorption mechanisms on gibbsite. *Soil Sci. Soc. Am. J.* **2014,** *78*, 473-479.

21. Park, C. M., Analysis of mercury adsorption at the gibbsite-water interface using the CD-MUSIC model. *Environ. Sci. Pollut. Res.* **2018,** *25*, 21721-21730.

22. Reynolds, J. G.; Cooke, G. A.; Herting, D. L.; Warrant, R. W., Evidence for dawsonite in Hanford high-level nuclear waste tanks. *J. Hazard. Mater.* **2012,** *209*, 186-192.

23. Restivo, M. L.; Stone, M. E.; Herman, D. T.; Duignan, M. R.; Smith, G. L.; Wells, B. E.; Lumetta, G. J.; Enderlin, C. W.; Adkins, H. E. *Technology Evaluation for Conditioning of Hanford Tank Waste using Solids Segregation and Size Reduction*; Pacific Northwest National Laboratory: 2014; p 65.

24. Reynolds, J. G.; McCoskey, J. K.; Herting, D. L., Gibbsite solubility in Hanford nuclear waste approached from above and below saturation. *Ind. Eng. Chem. Res.* **2016,** *55*, 5465-5473.

25. Shen, Z. Z.; Ilton, E. S.; Prange, M. P.; Kerisit, S. N., Molecular dynamics simulations of the interfacial region between boehmite and gibbsite basal surfaces and high ionic strength aqueous solutions. *J. Phys. Chem. C* **2017,** *121*, 13692-13700.

26. Baumann, N.; Brendler, V.; Arnold, T.; Geipel, G.; Bernhard, G., Uranyl sorption onto gibbsite studied by time-resolved laser-induced fluorescence spectroscopy (TRLFS). *J. Colloid Interface Sci.* **2005,** *290*, 318-324.

27. Chang, H.-S.; Korshin, G. V.; Wang, Z.; Zachara, J. M., Adsorption of uranyl on gibbsite: A time-resolved laser-induced fluorescence spectroscopy study. *Environ. Sci. Technol.* **2006,** *40*, 1244-1249.

28. Hattori, T.; Saito, T.; Ishida, K.; Scheinost, A. C.; Tsuneda, T.; Nagasaki, S.; Tanaka, S., The structure of monomeric and dimeric uranyl adsorption complexes on gibbsite: A combined DFT and EXAFS study. *Geochim. Cosmochim. Acta* **2009,** *73*, 5975-5988.

29. Gückel, K.; Rossberg, A.; Brendler, V.; Foerstendorf, H., Binary and ternary surface complexes of U(VI) on the gibbsite/water interface studied by vibrational and EXAFS spectroscopy. *Chem. Geol.* **2012,** *326*, 27-35.

30. Gückel, K.; Rossberg, A.; Müller, K.; Brendler, V.; Bernhard, G.; Foerstendorf, H., Spectroscopic identification of binary and ternary surface complexes of Np(V) on gibbsite. *Environ. Sci. Technol.* **2013,** *47*, 14418-14425.

31. MacKenzie, R. C.; Meldau, R.; Gard, J. A., The ageing of sesquioxide gels: II. Alumina gels. *Mineral. Mag.* **1962,** *33*, 145-157.

32. McHardy, W. J.; Thomson, A. P., Conditions for the formation of bayerite and gibbsite. *Mineral. Mag.* **1971,** *38*, 358-368.

33. Halfon, A.; Kaliaguine, S., Alumina-trihydrate crystallization .1. Secondary nucleation and growth-rate kinetics. *Can. J. Chem. Eng.* **1976,** *54*, 160-167.

34. Halfon, A.; Kaliaguine, S., Alumina-trihydrate crystallization .2. Model of agglomeration. *Can. J. Chem. Eng.* **1976,** *54*, 168-172.

35. Freij, S. J.; Parkinson, G. M.; Reyhani, M. M., Atomic force microscopy study of the growth mechanism of gibbsite crystals. *Phys. Chem. Chem. Phys.* **2004,** *6*, 1049-1055.

36. Brown, N., Crystal growth and nucleation of aluminium trihydroxide from seeded caustic aluminate solutions. *J. Cryst. Growth* **1972,** *12*, 39-45.

37. Lloyd, S.; Thurgate, S. M.; Cornell, R. M.; Parkinson, G. M., Atomic force microscopy of gibbsite. *Appl. Surf. Sci.* **1998,** *135*, 178-182.

38. Seyssiecq, I.; Veesler, S.; Boistelle, R.; Lamerant, J. M., Agglomeration of gibbsite $Al(OH)_3$ crystals in Bayer liquors. Influence of the process parameters. *Chem. Eng. Sci.* **1998,** *53*, 2177-2185.

39. Freij, S. J.; Parkinson, G. M.; Reyhani, M. M., Direct observation of the growth of gibbsite crystals by atomic force microscopy. *J. Cryst. Growth* **2004,** *260*, 232-242.

40. Zhang, X.; Zhang, X. W.; Graham, T. R.; Pearce, C. I.; Mehdi, B. L.; N'Diaye, A. T.; Kerisit, S.; Browning, N. D.; Clark, S. B.; Rosso, K. M., Fast synthesis of gibbsite nanoplates and process optimization using Box-Behnken experimental design. *Cryst. Growth Des.* **2017,** *17*, 6801-6808.

41. Webster, N. A. S.; Loan, M. J.; Madsen, I. C.; Knott, R. B.; Brodie, G. M.; Kimpton, J. A., An in situ synchrotron X-ray diffraction investigation of lepidocrocite and ferrihydrite-seeded $Al(OH)_3$ crystallisation from supersaturated sodium aluminate liquor. *J. Cryst. Growth* **2012,** *340*, 112-117.

42. Nagy, K. L.; Cygan, R. T.; Hanchar, J. M.; Sturchio, N. C., Gibbsite growth kinetics on gibbsite, kaolinite, and muscovite substrates: Atomic force microscopy evidence for epitaxy and an assessment of reactive surface area. *Geochim. Cosmochim. Acta* **1999,** *63*, 2337-2351.

43. Lee, S. S.; Schmidt, M.; Fister, T. T.; Nagy, K. L.; Sturchio, N. C.; Fenter, P., Structural characterization of aluminum (oxy)hydroxide films at the muscovite (001)−water interface. *Langmuir* **2016,** *32*, 477-486.

44. Sillanpaa, A. J.; Paivarinta, J. T.; Hotokka, M. J.; Rosenholm, J. B.; Laasonen, K. E., A computational study of aluminum hydroxide solvation. *J. Phys. Chem. A* **2001,** *105*, 10111-10122.

45. Buvari-Barcza, A.; Rozsahegyi, M.; Barcza, L., Hydrogen bonded associates in the Bayer process (in concentrated aluminate lyes): the mechanism of gibbsite nucleation. *J. Mater. Chem.* **1998,** *8*, 451-455.

46. Gale, J. D.; Rohl, A. L.; Watling, H. R.; Parkinson, G. M., Theoretical investigation of the nature of aluminum-containing species present in alkaline solution. *J. Phys. Chem. B* **1998,** *102*, 10372-10382.

47. Sarpola, A.; Hietapelto, V.; Jalonen, J.; Jokela, J.; Laitinen, R. S.; Ramo, J., Identification and fragmentation of hydrolyzed aluminum species by electrospray ionization tandem mass spectrometry. *J. Mass Spectrom.* **2004,** *39*, 1209-1218.

48. Sarpola, A.; Hietapelto, V.; Jalonen, J.; Jokela, J.; Laitinen, R. S., Identification of the hydrolysis products of $AlCl_3 \cdot 6H_2O$ by electrospray ionization mass spectrometry. *J. Mass Spectrom.* **2004,** *39*, 423-430.

49. Saukkoriipi, J.; Laasonen, K., Theoretical study of the hydrolysis of pentameric aluminum complexes. *J. Chem. Theory Comput.* **2010,** *6*, 993-1007.

50. Lee, S. S.; Fenter, P.; Park, C.; Nagy, K. L., Fulvic acid sorption on muscovite mica as a function of pH and time using in-situ X-ray reflectivity. *Langmuir* **2008,** *24*, 7817-7829.

51. Lee, S. S.; Nagy, K. L.; Park, C.; Fenter, P., Enhanced uptake and modified distribution of mercury(II) by fulvic acid on the muscovite (001) surface. *Environ. Sci. Technol.* **2009,** *43*, 5295-5300.

52. Schlegel, M. L.; Nagy, K. L.; Fenter, P.; Cheng, L.; Sturchio, N. C.; Jacobsen, S. D., Cation sorption on the muscovite (001) surface in chloride solutions using high-resolution X-ray reflectivity. *Geochim. Cosmochim. Acta* **2006,** *70*, 3549-3565.

53. Pintea, S.; de Poel, W.; de Jong, A. E. F.; Vonk, V.; van der Asdonk, P.; Drnec, J.; Balmes, O.; Isern, H.; Dufrane, T.; Felici, R.; Vlieg, E., Solid–liquid interface structure of muscovite mica in CsCl and RbBr solutions. *Langmuir* **2016,** *32*, 12955-12965.

54. Brugman, S. J. T.; Townsend, E. R.; Smets, M. M. H.; Accordini, P.; Vlieg, E., Concentration-dependent adsorption of CsI at the muscovite-electrolyte interface. *Langmuir* **2018,** *34*, 3821-3826.

55. Nagy, K. L.; Lasaga, A. C., Dissolution and precipitation kinetics of gibbsite at 80ºC and pH 3: The dependence on solution saturation state. *Geochim. Cosmochim. Acta* **1992,** *56*, 3093-3111.

56. Bethke, C. M.; Yeakel, S., The Geochemist's Workbench: Reference Manual. Aqueous Solutions, LLC: Champaign, 2013.

57. Fenter, P. A., X-ray reflectivity as a probe of mineral-fluid interfaces: A user guide. In *Application of Synchrotron Radiation in Low-Temperature Geochemistry and Environmental Science, Reviews in Mineralogy and Geochemistry*, Fenter, P. A.; Rivers, M. L.; Sturchio, N. C.; Sutton, S. R., Eds. Geochemical Society and Mineralogical Society of America: Washington DC, 2002; Vol. 49, pp 149-220.

58. Cheng, L.; Fenter, P.; Nagy, K. L.; Schlegel, M. L.; Sturchio, N. C., Molecular-scale density oscillations in water adjacent to a mica surface. *Phys. Rev. Lett.* **2001,** *87*, 156103-1-4.

59. Wilson, A. J. C., *International Tables for Crystallography, vol. C: Mathematical, Physical, and Chemical Tables*. Dordrecht: Kluwer Academic Publishers: Dordrecht, 1992; p 500-503.

60. Lee, S. S.; Park, C.; Fenter, P.; Sturchio, N. C.; Nagy, K. L., Competitive adsorption of strontium and fulvic acid at the muscovite-solution interface observed with resonant anomalous X-ray reflectivity. *Geochim. Cosmochim. Acta* **2010,** *74*, 1762-1776.

61. Fenter, P.; Sturchio, N. C., Mineral–water interfacial structures revealed by synchrotron X-ray scattering. *Prog. Surf. Sci.* **2004,** *77*, 171-258.

62. Lee, S. S.; Fenter, P.; Nagy, K. L.; Sturchio, N. C., Monovalent ion adsorption at the muscovite (001) - solution interface: Relationships among ion coverage and speciation, interfacial water structure, and substrate relaxation. *Langmuir* **2012,** *28*, 8637-8650.

63. Lee, S. S.; Fenter, P.; Park, C.; Sturchio, N. C.; Nagy, K. L., Hydrated cation speciation at the muscovite (001)-water interface. *Langmuir* **2010,** *26*, 16647-16651.

64. Lee, S. S.; Schmidt, M.; Laanait, N.; Sturchio, N. C.; Fenter, P., Investigation of adsorbed structure, adsorption free energy, and overcharging behavior of trivalent yttrium at the muscovite (001)-water interface. *J. Phys. Chem. C* **2013,** *117*, 23738-23749.

65. Baes, C. F.; Mesmer, R. E., *The Hydrolysis of Cations*. Wiley Interscience: New York, 1976.

66. Clearfield, A., The mechanism of hydrolytic polymerization of zirconyl solutions. *J. Mater. Res.* **1990,** *5*, 161-162.

67. Navrotsky, A., Energetic clues to pathways to biomineralization: Precursors, clusters, and nanoparticles. *Proc. Natl. Acad. Sci. USA* **2004,** *101*, 12096-12101.

68. De Yoreo, J. J.; Gilbert, P. U. P. A.; Sommerdijk, N. A. J. M.; Penn, R. L.; Whitelam, S.; Joester, D.; Zhang, H.; Rimer, J. D.; Navrotsky, A.; Banfield, J. F.; Wallace, A. F.; Michel, F. M.; Meldrum, F. C.; Cölfen, H.; Dove, P. M., Crystallization by particle attachment in synthetic, biogenic, and geologic environments. *Science* **2015,** *349*, aaa6760.

69. Park, C.; Fenter, P. A.; Sturchio, N. C.; Nagy, K. L., Thermodynamics, interfacial structure, and pH hysteresis of Rb^+ and Sr^{2+} adsorption at the muscovite (001)-solution interface. *Langmuir* **2008,** *24*, 13993-14004.

70. Bloom, P. R.; Erich, M. S., Effect of solution composition on the rate and mechanism of gibbsite dissolution in acid solutions. *Soil Sci. Soc. Am. J.* **1987,** *51*, 1131-1136.

71. Ham, Y.-S.; Okazaki, M.; Suzuki, S.; Nakagawa, N., Determination of total aluminum concentration in soil solution using capillary electrophoresis. *J. Soil Sci. Plant Nutr.* **2003,** *49*, 9-16.

72. Liu, Y. T.; Wang, M. K.; Chen, T. Y.; Chiang, P. N.; Huang, P. M.; Lee, J. F., Arsenate sorption on lithium/aluminum layered double hydroxide intercalated by chloride and on gibbsite: Sorption isotherms, envelopes, and spectroscopic studies. *Environ. Sci. Technol.* **2006,** *40*, 7784-7789.

73. Rosenqvist, J.; Persson, P.; Sjöberg, S., Protonation and charging of nanosized gibbsite (α-$Al(OH)_3$) particles in aqueous suspension. *Langmuir* **2002,** *18*, 4598-4604.

74. Liu, X.; Cheng, J.; Sprik, M.; Lu, X.; Wang, R., Understanding surface acidity of gibbsite with first principles molecular dynamics simulations. *Geochim. Cosmochim. Acta* **2013,** *120*, 487-495.

75. Gan, Y.; Franks, G. V., Charging behavior of the gibbsite basal (001) surface in NaCl solution investigated by AFM colloidal probe technique. *Langmuir* **2006,** *22*, 6087-6092.

Table of Contents (TOC) Graphic (Review Only)